Global Cancer Risk from Unregulated Polycyclic Aromatic Hydrocarbons

Jamie M. Kelly[1,*], Peter D. Ivatt[2], Mathew J. Evans[2,3], Jesse H. Kroll[4], Amy I. H. Hrdina[4], Ishwar N. Kohale[5,6], Forest M. White[5,6,7], Bevin P. Engelward[7], and Noelle E. Selin[1,8,*]

[1]Institute for Data, Systems, and Society, Massachusetts Institute of Technology, MA, 02139, USA.

[2]Wolfson Atmospheric Chemistry Laboratories, Department of Chemistry, University of York, York, YO10 5DD, UK.

[3]National Centre for Atmospheric Science, Wolfson Atmospheric Chemistry Laboratories, University of York, YO10 5DD, UK.

[4]Department of Civil and Environmental Engineering, Massachusetts Institute of Technology, Cambridge, MA, 02139, USA.

[5]Department of Biological Engineering, Massachusetts Institute of Technology, Cambridge, MA, 02139, USA.

[6]David H. Koch Institute for Integrative Cancer Research, Massachusetts Institute of Technology, Cambridge, MA, 02139, USA.

[7]Center for Precision Cancer Medicine, Massachusetts Institute of Technology, Cambridge, MA, 02139, USA.

[8]Department of Earth, Atmospheric and Planetary Sciences, Massachusetts Institute of Technology, Cambridge, MA, 02139, USA.

Corresponding authors(*): Jamie M. Kelly (jamiekel@mit.edu) and Noelle E. Selin (selin@mit.edu)

Key Points:

- Benzo[a]pyrene is a small contributor to human cancer risk of PAHs worldwide (11 %)
- Using benzo[a]pyrene as a surrogate compound leads to erroneous conclusions about high-risk populations and the importance of uncertain chemical processes
- Science and policy could be improved by considering a wider group of both emitted PAHs as well as their degradation products

Abstract

Scientists and regulators commonly use benzo[a]pyrene concentrations to assess cancer risk from complex mixtures of atmospheric polycyclic aromatic hydrocarbons (PAHs). Here, we show that benzo[a]pyrene is a poor indicator of PAH risk distribution and management: nearly 90% of cancer risk worldwide results from other PAHs, including unregulated degradation products of emitted PAHs. We develop and apply a global-scale atmospheric model and conduct health impact analyses to estimate human cancer risk from 16 PAHs and their N-PAH degradation products. We find that benzo[a]pyrene is a minor contributor to the total cancer risks of PAHs (11%); the remaining risk comes from other directly-emitted PAHs (73%) and N-PAHs (15%). We show that assessment and policy-making that relies solely on benzo[a]pyrene exposure provides misleading estimates of risk distribution, the importance of chemical processes, and the prospects for risk mitigation. We conclude that researchers and decision-makers should consider additional PAHs as well as degradation products.

Plain Language Summary

Nearly 90% of global human lung cancer risk from polycyclic aromatic hydrocarbons (PAHs) comes from compounds omitted by prior analyses and not regulated directly. PAHs in the atmosphere are a complex mixture, but regulators and researchers often represent them using a single compound, benzo(a)pyrene. We show that benzo(a)pyrene is a poor indicator of global PAH cancer risk; its use as a proxy leads to erroneous conclusions about high-risk populations and atmospheric chemical processes. 15% of risk comes from PAHs that are produced in atmospheric reactions and are not regulated or routinely monitored. Regulators and researchers should focus on the entire mixture of PAHs in the atmosphere, and we recommend that benzo(a)pyrene not be used as a sole reference compound.

1 Introduction

Polycyclic aromatic hydrocarbons (PAHs) are a class of chemicals that contain multiple fused aromatic rings, and are emitted into the atmosphere as byproducts of burning organic matter (Keyte et al., 2013). Several PAHs have been identified as mutagenic or carcinogenic (Bostrom et al., 2002) and therefore have the potential to harm the health of humans (Hansen et al., 2007; Park & Park, 2009) and ecosystems (Gray, 2002). In the atmosphere, PAHs are present as a complex mixture, with different people inhaling different combinations of these carcinogens (Dixon et al., 2019). However, scientific research and environmental guidelines often represent this complex PAH mixture using a single surrogate compound, benzo[a]pyrene (BAP).

Epidemiological (Armstrong et al., 2004; Moolgavkar et al., 1998) and animal (Collins et al., 1991; Heinrich et al., 1994; Thyssen et al., 1981) studies have been used to estimate the cancer risk of human exposure to BAP, even though humans are exposed to many different kinds of PAHs. Risk estimates derived from epidemiological studies imply that exposure of 1 ng m^{-3} of BAP to a population of 1 million people will induce 230-830 cancer cases over their lifetime (~70 years). This is equivalent to an epidemiologically-derived unit risk (UR_E) that ranges 213-850 $x10^{-6}$ per (ng/m^3) (Armstrong et al., 2004; Moolgavkar et al., 1998). Existing epidemiological studies have not accounted for the confounding exposure to other PAHs, or exposure to other pollutants such as heavy metals, sulphur dioxide and nitrogen oxide. Cancer

risks derived from studies in which animals were exposed to BAP alone are lower than those derived from epidemiological studies (UR_A = 0.3-1.7 $x10^{-6}$ per (ng/m^3)) (Collins et al., 1991; Thyssen et al., 1981) suggesting an increased risk associated with other components of PAH mixtures.

Scientific research and environmental guidelines nearly always use BAP as an indicator for calculating risk from the entire PAH mixture. Shen et al. (2014) and Shrivastava et al. (2017) estimate global-average human lung cancer risks of 20-31 $x10^{-6}$ by combining global-scale models of BAP in the atmosphere with an epidemiologically-derived BAP unit risk - however, although estimates of UR_E vary by a factor of ~4, both Shen et al. (2014) and Shrivastava et al. (2017) test only the upper limit of this value. By using BAP as the sole indicator, these studies also assume that variations in BAP concentrations reflect proportional variations in risk. While PAHs are regulated as a class of substances, national and international governing bodies also use BAP as an indicator for all species: BAP is the only PAH to have a guideline concentration. In studies where multiple PAHs are considered, BAP is estimated as the major contributor to the cancer risk of PAHs (40-80%)(Delgado-Saborit et al., 2011; Nielsen et al., 1996; Norramit et al., 2005; Zhang et al., 2016; Zhang et al., 2009), but many of those studies do not include highly toxic emitted PAHs (e.g. dibenz[a,h]anthracene), and none include degradation products.

Recent work suggests that the atmospheric degradation products of PAHs, such as those containing a nitro group (-NO_2) that we refer to here as N-PAHs, are highly toxic, but their impact on human health remains uncertain. N-PAHs, including both nitro-PAHs (one -NO_2 group) and dinitro-PAHs (two -NO_2 groups), can be up to 1,000 times more toxic than their respective parent compound (Wislocki et al., 1986). Laboratory studies have shown that N-PAHs are formed under several different oxidation reactions in the atmosphere (Keyte et al., 2013). N-PAHs have been detected in a variety of environments, from urban(Albinet et al., 2007; Elzein et al., 2019) to remote (Drotikova et al., 2020; Lammel et al., 2017). The chemical formation of N-PAHs in the atmosphere has been simulated in regional-scale (Mulder et al., 2019) and global-scale (Wilson, 2020) atmospheric modelling studies; those studies, however, did not include a key particle-phase reaction with the nitrate radical (NO_3) that laboratory studies suggest could be an extremely efficient source of N-PAHs (Zelenov et al., 2018; Zhang et al., 2014). Furthermore, as prior studies did not perform human health impact assessments, the importance of N-PAHs in the context of human health, as well as in relation to other advancements in this field, are both unknown.

Researchers in previous studies have argued that uncertainties in heterogeneous oxidation kinetics (Poschl et al., 2001; Zhou et al., 2019; Zhou et al., 2013) and gas-particle partitioning (Dachs & Eisenreich, 2000; Shahpoury et al., 2016) have a large effect on exposure and human health impacts of BAP, but the importance of these uncertain processes in the context of other emitted PAHs and degradation products remains unknown. Shrivastava et al. (2017) found that reducing the rate of BAP heterogeneous oxidation resulted in a four-fold increase in estimated human exposure to BAP, and a five-fold increase in PAH human cancer risk when using BAP as an indicator of health risks. However, reductions in the oxidation rate will also diminish human exposure to degradation products, which may themselves be toxic – this effect was not considered by Shrivastava et al. (2017), who used BAP concentrations as a proxy for overall PAH exposure and risk. Additional studies (Friedman et al., 2014; Friedman & Selin, 2012; Friedman et al., 2014; Mu et al., 2018; Thackray et al., 2015) have advanced understanding of PAH chemistry in the atmosphere through simulations of 1-3 PAH species. The sensitivity of

process-based conclusions to the inclusion of additional PAHs and degradation products remains unassessed.

Here, we reevaluate the importance of BAP and its suitability as an indicator compound for global-scale cancer risk of PAHs, and we perform a bounding exercise to assess how uncertainties in concentrations and atmospheric processes affect conclusions drawn in previous studies which were based on BAP alone. To do this, we develop and use a global-scale atmospheric chemistry model to estimate concentrations of PAHs in the atmosphere, and use human health impact analyses to estimate the human cancer risk associated with atmospheric PAHs, using traditional epidemiologically-based functions as well as a novel framework based on toxicity data from animal studies which allows us to explicitly estimate the risks of individual components of the PAH mixture. In contrast to previous global-scale modeling studies which typically considered only BAP (Friedman et al., 2014; Friedman & Selin, 2012; Friedman et al., 2014; Lammel et al., 2009; Mu et al., 2018; Octayiani et al., 2019; Shen et al., 2014; Shrivastava et al., 2017; Thackray et al., 2015), we account for the 16 PAHs identified as priority pollutants by the United Stated Environmental Protection Agency ("USEPA16") as well as N-PAH degradation products. We quantify the sensitivity of estimates of global cancer risk to (i) inclusion of additional PAHs, (ii) gas-particle partitioning, (iii) heterogeneous oxidation kinetics, and (iv) model resolution. We conclude that BAP accounts for only a small fraction of the human cancer risk of PAHs globally, while the N-PAHs, which are unregulated and commonly omitted by measurement and modeling studies focused on the atmosphere, are a potentially large source of carcinogenic risk. We also find that atmospheric kinetic and partitioning uncertainties have a much lower impact on risk magnitudes than was identified in previous studies. We suggest that future research and regulatory guidelines explicitly consider a broader range of PAHs and their degradation products in assessments of cancer risk from these compounds.

2 Materials and Methods

2.1 Experimental Design

We provide a total of fourteen estimates of global human cancer risk from PAHs by combining seven different PAH concentration distributions from a global-scale atmospheric chemistry model, with two distinct methods for estimating human cancer risk. Together, this analysis allows us to quantify the suitability of BAP as an indicator of risk of PAH mixtures, and to bound the importance of contributors to uncertainty.

2.2 Description of Atmospheric Chemistry Model (GOES-Chem)

We use a numerical, three-dimensional, atmospheric chemistry model, GEOS-Chem (Bey et al., 2001; http://acmg.seas.harvard.edu/geos/) version 11. We perform model simulations at a two different horizontal resolutions, of 4° x 5° and 2° x 2.5° – both with 47 vertical levels, extending from the surface of the Earth to ~80 km altitude. Meteorological fields are driven by MERRA-2 reanalysis from the NASA Global Modeling and Assimilation Office (Global Modeling and

Assimilation Office, GMAO). We use the "tropchem" chemical mechanism (Eastham et al., 2014) for this work, which includes a detailed and fully coupled treatment of HOx –NO_X –VOC–O_3 and a bulk aerosol scheme with fixed log-normal modes. Aerosol components considered include sulfate, sea salt, black carbon, mineral dust and organic carbon. Inorganic aerosol thermodynamics are calculated using ISORROPIA (Fountoukis & Nenes, 2007). Both OC and BC are further separated into hydrophilic and hydrophobic components. The tropchem mechanism is expanded to also consider PAHs (described below – 2.3). Dry deposition of both gases and aerosol are parameterized in a scheme which applies a resistance-in-series approach (Wesely, 1989; Zhang et al., 2001). Wet deposition occurs both within and below clouds, and is dependent on the species-specific effective Henry's Law constant (Amos et al., 2012). These model simulations use a variety of different global and regional-scale emission inventories for non-PAH species. Global-scale emission inventories used here for non-PAH species include EDGAR (Crippa et al., 2018) and RETRO (Hu et al., 2015). Where necessary, these global-scale emission inventories are overwritten with regional-scale emission inventories - e.g. NEI over USA (Travis et al., 2016), EMEP over Europe (van Donkelaar et al., 2008). For biomass burning and biogenic emissions, we use GFED4 (Giglio et al., 2013) and MEGAN (Guenther et al., 2012), respectively. Emissions of PAHs are discussed in greater detail in the following section. In the next sections, we describe how PAHs are simulated within the GEOS-Chem model, highlighting new developments.

2.3 Treatment of PAHs and N-PAHs in GEOS-Chem

The GEOS-Chem model has previously been used to examine PAH chemistry and transport in the atmosphere, both for the present day(Friedman et al., 2014; Friedman & Selin, 2012; Thackray et al., 2015) and future climate simulations (Friedman et al., 2014). We extend the model (Friedman & Selin, 2012) such that PAHs are now fully interactive with other atmospheric species. This allows a two-way chemical feedback between PAHs and all other gaseous and aerosol species. Previous simulations used an offline version of the model, whereby gas and aerosol concentrations from the 'full' chemistry simulation were archived and used as input for the PAH simulation.

Whereas previous modelling studies only consider between 1 and 3 PAHs, we extend the GEOS-Chem model to provide global-scale concentration information for a total of 48 PAH species. This consists of 16 emitted PAHs; the US EPA's list of priority PAHs. These include naphthalene (NAP), acenaphthylene (ACY), acenaphthene (ACE), fluorene (FLU), phenanthrene (PHEN), anthracene (ANT), fluoranthene (FLA), pyrene (PYR), benzo[a]anthracene (BAA), chrysene (CHR), benzo[b]fluoranthene (BBF), benzo[k]fluoranthene (BKF), benzo[a]pyrene (BAP), benzo[g,h,i]perylene (BGHIP), indeno[1,2,3-c,d]pyrene (ICDP), and dibenz[a,h]anthracene (DAHA). The remaining 32 PAH species are the corresponding nitro-PAHs (x16) and dinitro-PAHs (x16).

Although commonly neglected from atmospheric modelling studies, we account for N-PAH formation in the atmosphere by building a chemical mechanism. We build a degradation mechanism of pyrene (PYR) that accounts for the formation of nitropyrene (nitro-PYR) and dinitropyrene (dinitro-PYR) (Table 1). This mechanism is generalized, as it is based on the

findings from laboratory studies which are not all on pyrene. We chose pyrene for three reasons. First, pyrene is the only species where N-PAH formation yields have been determined in laboratory studies for each reaction pathway. Second, N-PYR is included in multiple field campaigns, allowing us to evaluate our predicted concentrations for this species. Many other N-PAHs have not been measured in the atmosphere. Third, the toxicity of N-PYR and DN-PYR are known, allowing us to quantify the human cancer risk of the oxidation products. The mechanism that describes the source and sinks for pyrene and its N-PAHs is displayed in Table 1. For this species, we account for the formation of nitropyrene via (i) gas-phase photooxidation, (ii) gas-phase direct nitration, and (iii) particle-phase direct nitration. Photolysis of the N-PYRs is also accounted for. For the remaining 15 emitted PAHs, the chemical mechanism only accounts for the chemical removal of the parent compound, and not the production of the N-PAHs. For these PAHs, we account for the major sinks (gas-phase photooxidation and particle-phase ozonolysis), without directly tracking the products of chemical mechanism online in GEOS-Chem. This way of representing PAHs (i.e. the processes considered, and the neglect of oxidation products), is consistent with previous global and regional scale modelling studies (e.g. Friedman et al. (2012)). N-PAH concentrations from these 15 emitted PAHs are estimated in our bounding exercise and uncertainty analyses by applying the spatial distributions in the N-PYR/PYR and DN-PYR/PYR ratios (Figure S2, SI) to concentrations of the remaining PAHs as a proxy for spatial patterns of their N-PAH products.

Table 1. Reaction kinetics for N-PAHs. Chemical and photolytic reactions of pyrene (PYR) included in the updated version of the chemical-transport model (GEOS-Chem).

		Reaction	2^{nd} order rate coefficient	Reference
Pyrene (PYR)	Gas-phase			
	R1.	$PYR_{(g)} + NO_3 \rightarrow NPYR$	1.6×10^{-27} x $[NO_2]$	(Atkinson et al.,1990; Keyte et al., 2013)
	R2.	$PYR_{(g)} + OH \rightarrow PYR\text{-}OH$	5.0×10^{-11}	(Atkinson et al., 1990)
	R3.	$PYR\text{-}OH + O_2 \rightarrow$ products	1.0×10^{-17}	(Koch et al., 2007) (from benzene)
	R4.	$PYR\text{-}OH + NO_2 \rightarrow NPYR$	3.6×10^{-11}	(Feilberg et al., 1999) (from naphthalene)
	Particle-phase			
	R6.	$PYR_{(p)} + NO_3 \rightarrow NPYR$	6.4×10^{-12}	(Liu et al., 2012)
	R7.	$PYR_{(p)} + O_3 \rightarrow$ products	4.27×10^{-17}	Mean = (Liu et al., 2012) and (Perraudin et al., 2007)
Nitropyrene (NPYR)	Gas-phase			
	R8.	$NPYR_{(g)} + NO_3 \rightarrow DNPYR$	1.6×10^{-27} x $[NO_2]$	Identical to PYR
	R9.	$NPYR_{(g)} + OH \rightarrow NPYR\text{-}OH$	5.0×10^{-11}	Identical to PYR
	R10.	$NPYR\text{-}OH + O_2 \rightarrow$ products	1.0×10^{-17}	(Koch et al., 2007) (from benzene)

	R11.	NPYR-OH + $NO_2 \rightarrow$ DNPYR	$3.6e\times10^{-11}$	(Feilberg et al., 1999) (from naphthalene)
	Particle-phase			
	R12.	$NPYR_{(p)} + NO_3 \rightarrow$ DNPYR	1.3×10^{-12}	(Liu et al., 2012)
	R13.	$NPYR_{(p)} + O_3 \rightarrow$ products	2.2×10^{-17}	(Miet et al., 2009)
	R14.	$NPYR_{(p)} + h\nu \rightarrow$ products	$1.3 – 5.0 \times10^{-4}$	
Dinitropyrene (DNPYR)	Gas-phase			
	R15.	$DNPYR_{(g)} + NO_3 \rightarrow$ products	5.0×10^{-11}	Identical to PYR
	R16.	$DNPYR_{(g)} + OH \rightarrow$ products	1.6×10^{-27} x $[NO_2]$	Identical to PYR
	Particle-phase			
	R17.	$DNPYR_{(p)} + NO_3 \rightarrow$ products	1.3×10^{-12}	Same as nitro-PYR
	R18.	$DPYR_{(p)} + O_3 \rightarrow$ products	2.2×10^{-17}	Same as nitro-PYR
	R19.	$DPYR_{(p)} + h\nu \rightarrow$ products	$1.3 – 5.0 \times10^{-4}$	

223

224 We provide two descriptions for heterogeneous oxidation kinetics which differ only by
225 their reaction rate coefficients, allowing us to quantify how uncertainty in the rate of this process
226 contributes to uncertainty in PAH distributions and human cancer risk. Within the GEOS-Chem
227 model, particle-phase ozonolysis kinetics follow the Arrhenius equation using a second-order
228 rate coefficient (k) from Perraudin et al. (2007). Although alternative laboratory studies show
229 that heterogeneous PAH oxidation follows a Langmuir-Hinshelwood type reaction mechanism,
230 implying that k is variable (dependent on ozone), the parameters required to account for these
231 more realistic descriptions of heterogeneous PAH oxidation kinetics have only been developed
232 for a limited number of PAHs, and are not implemented in this study. However, as we know this
233 process could be much slower, we conduct a sensitivity simulation where k is reduced to 10 % of
234 its laboratory-derived value.

235 We implement two widely-used approaches to estimate gas-particle partitioning, allowing
236 us to bound the importance of uncertainties associated with this process. PAHs are semi-volatile,
237 meaning they can partition between gas and particle phases. In the particle-phase, PAHs are
238 observed to either be absorbed within organic aerosol (OA), or adsorbed onto the surface of
239 black carbon (BC). We chose to implement a poly parameter linear free energy (Shahpoury et al.,
240 2016) (ppLFER) scheme, but for comparison, we also conduct simulations using a single
241 parameter scheme following Dachs and Eisenreich (Dachs & Eisenreich, 2000) (D&E).

242 PAH emissions for the year 2014 are from the global-scale emission inventory developed
243 by Shen et al. (2013). This emission inventory is used widely across global-scale atmospheric
244 modelling studies (Friedman et al., 2014; Friedman & Selin, 2012; Mu et al., 2018; Shrivastava
245 et al., 2017; Thackray et al., 2015). The combined USEPA16 global-total annual-total emission
246 rate is 504 Gg a^{-1}, with an interquartile range of 331-818 Gg a^{-1} (Shen et al., 2013) The sectors
247 included in this inventory are residential and commercial, industry, transportation, deforestation,
248 agriculture, and energy production.

249 Gas-phase PAHs undergo dry and wet deposition in a similar fashion to other gases. For
250 all gas-phase species, we assign a Henry's Law solubility constant of 3.1×10^{-5} m^3 atm^{-1} mol^{-1},
251 taken from Sander (2015) (Sander, 2015). Particle-phase PAHs are assumed to undergo dry and
252 wet deposition according to the aerosol that it is bound to – that is, dry and wet deposition
253 parameters describing the aerosol particle are used to describe deposition of the particle-phase
254 PAH.

255

256 2.4 GEOS-Chem Model Simulations Performed in Study

257 We perform four global-scale model simulations, which are presented in Table 2. For all
258 simulations, we discard the first month of simulation as spin up, and base our analysis on the
259 remaining 12 months: January 2014 – December 2014. For the base simulation, we use 4° x 5°
260 horizontal resolution, second order rate coefficients describing heterogeneous oxidation kinetics
261 are taken directly from the laboratory studies, and gas-particle partitioning follows the ppLFER
262 scheme. We then perform three sensitivity simulations, where we change one parameter at a

263 time, allowing us to isolate the importance of uncertainties in each of these processes. In the first
264 sensitivity simulation, we reduce the heterogeneous oxidation rate coefficient to 10 % of its
265 original value ('Het_0.1'; Table 2). In the second sensitivity simulation, we change the gas-
266 particle partitioning scheme from the ppLFER to the D&E scheme ('D&E'; Table 2). In the third
267 sensitivity simulation, we change the model horizontal resolution from 4° x 5° to 2° x 2.5°
268 horizontal ('2x2.5'; Table 2).

269

270 **Table 2**. Overview of GEOS-Chem model simulations performed in in this study. Note, whereas
271 the first four simulations in table are unique model simulations, the final three simulations are
272 based on the Base simulation, but with various bias-correction techniques applied.

Simulations	Gas-particle partitioning	Gas-particle partitioning scheme	Resolution	Bias-correction
Base	Laboratory-derived	ppLFER	4° x 5°	None
Het_0.1	10 % of laboratory value	ppLFER	4° x 5°	None
D&E	Laboratory-derived	D&E	4° x 5°	None
2x2.5	10 % of laboratory value	ppLFER	2° x 2.5°	None
PAH_Corr	Laboratory-derived	ppLFER	4° x 5°	Corrected to PAH concentrations from
N-PAH_Min	Laboratory-derived	ppLFER	4° x 5°	Corrected to minimum N-PAH yields
N-PAH_Max	Laboratory-derived	ppLFER	4° x 5°	Corrected to maximum N-PAH yields

273

274 2.5 Observations Used to Evaluate Simulated PAHs and Provide Simple Bias-Corrections

275 We use observations to evaluate performance of the four aforementioned GEOS-Chem model
276 simulations, and also to provide three additional 'bias-corrected' PAH concentration
277 distributions (from the Base simulation.) Observations for Europe and North America were taken
278 from continuously-monitoring air quality networks Environmental Protection Agency, Air
279 Toxics and the European Monitoring and Evaluation Programme (EMEP) (accessed via the
280 Norwegian Institute for Air Research) and those for continental Asia (Saha et al., 2017), Asia-
281 Arctic ship cruise transect (Ma et al., 2013), and Africa (Klánová et al., 2008) are from field
282 campaigns. We apply three different 'bias corrections' to the PAH distributions from the base
283 simulation. To test for the effects of a bias in the differences in concentrations across the
284 different PAHs, we multiplied the simulated PAH concentrations by the average bias between
285 the simulated and observed mean PAH concentration across the non-urban sites (these bias-
286 correction factors are shown in Table S2, SI). To test for potential biases in simulated N-
287 PAH/PAH yields, we scaled the model-derived N-PAH/PAH ratio by the maximum/minimum

bias between the simulated and observed N-PAH/PAH (these scaling factors are shown in Table S3, SI). This provided upper and lower bound estimates for N-PAH formation potential.

2.6 Calculation of Incremental Lifetime Cancer Risk

We estimate the incremental lifetime cancer risk using two different methods. We combine these methods with PAH distributions from the four model simulations and three bias corrected model simulations, leading to a total of fourteen different estimates of ILCR.

In the epidemiologically-based method, we estimate ILCR (unitless) following

$$ILCR = UR_E \times [BAP]$$

Where UR_E is the epidemiologically-derived BAP unit-risk (unit = per (ng/m^3)), which is estimated at 21.3 (Moolgavkar et al., 1998), 32.7 (Armstrong et al., 2004), 85.0 (Armstrong et al., 2004) x10^{-6} per (ng/m^3), and [BAP] is the atmospheric concentration (ng/m^3) of BAP, which is derived from the model. Under this method, overall ILCR is assumed to scale directly with BAP concentrations, and the impacts of the entire PAH mixture are accounted for (but the mixture is assumed to be fixed across the world).

We also develop an animal-based method for estimating ILCR, which allows us to compare the human cancer risk of individual PAH species without double counting. This is calculated following

$$ILCR = \sum UR_A \times [PAH] \times TEQ$$

Where UR_A is the animal-derived BAP unit risk (unit = per (ng/m^3)), which is estimated estimated by Collins et al., (1991) at 0.37 1.0, or 1.7 x10^{-6} per (ng/m^3), $[PAH]$ is the atmospheric concentration (ng/m^3) of PAHs, and TEQ are their toxic equivalent quotients (unitless). Where possible, we use estimates of TEQ from the primary literature, which have not been rounded to the nearest significant figure or order of magnitude, as is the case in many literature reviews; this rounding would introduce additional uncertainty in the relative importance of different PAHs. However, where the primary literature is not available, we use the recommended values from the literature reviews. TEQ used in this study from the literature are shown in Table 3. We use the terms TEQ and Relative Potency Factor (RPF) interchangeably. This method assumes that the cancer risk of individual PAHs combines linearly, as there is no conclusive evidence to suggest otherwise. This animal-based method only includes the cancer risk of PAHs for which both exposure concentrations and toxicity information were available (28 of the 48 species: all 16 emitted of the emitted PAHs, 6 out of the 16 nitro-PAHs, and 6 out of the 16 dinitro-PAHs). When attributing ILCR to different PAHs in the animal-based method, we also account for possible biases in the simulated distribution of PAHs (i.e. differences in concentrations among different PAH species). To account for the effect of possible biases, we used the 'bias-corrected' spatial distributions of PAHs concentrations (see Table S1 in the SI for scaling factors). We also test for any biases in our predicted N-PAH/PAH ratios by performing sensitivity calculations, where these ratios are scaled using observed values (see Table S2 in the SI for scaling factors).

In the two equations above, the unit for the ILCR is cancer risk, and therefore dimensionless. We can combine these risks with gridded human population density and assume a human lifetime of 70 years to express the ILCR in the form of cancer rates per year. Gridded human population density is taken from the Socioeconomic Data and Applications Center (SEDAC).

Across both methods for estimating ILCR, we test minimum, median and maximum values of BAP toxicity (UR) from the literature. We also used both the epidemiological and animal-based methods to evaluate how uncertainties in heterogeneous oxidation kinetics affect estimates of PAH cancer risk, by applying them to two model simulations which differ in the reactivity of particle-phase PAHs. In the discussion, we provide a more detailed evaluation of advantages and disadvantages in the epidemiological- and animal-based methods for estimating ICRL.

Table 3. Relative toxicity of PAHs (TEQ). These values are used in the animal-based method for estimating ILCR. Note, we use the terms TEQ and RPF interchangeably. a = Nisbet & Lagoy (1992), b = Busby et al. (1989), c = Wislocki et al. (1986), d = Deutschwenzel et al. (1983), e = Fu et al. (1998), f = EPA (2009).

	PAH	Nitro-PAH	Dinitro-PAH
NAP	0.001[a]		
ACY	0.001[a]		
ACE	0.001 [a]		
FLO	0.00075 [a]		
PHE	0.00075 [a]		
ANT	0.155 [a]		
FLA	0.052 [b]	0.13 [b]	0.13 (assumed)
PYR	0.065 [c]	0.1 [c]	5.1 [c]
BAA	0.35 [c]	0.1 [c]	0.1 (assumed)
CHR	0.011 [b]	10.8 [c]	10.8 (assumed)
BBF	0.210000		
BKF	0.03 [d]		
BAP	-	0.47 [c]	0.47 (assumed)
ICDP	0.08 [d]		
DAHA	3.0 [e]		
BGHIP	0.01 [f,b]		

3 Results

3.1 Global and Regional Concentrations of Emitted PAHs

We evaluate model performance of simulating 16 emitted PAHs by comparing simulated and observed PAH concentrations in a variety of environments. Simulated PAH concentrations were compared to a variety of different measurements and are displayed in Figures 1. In Figure 1, the simulated annual average surface concentrations for three illustrative PAHs are shown, and observed values are overlaid (circles). The left column shows three emitted PAHs, which are discussed in this section. The right column shows an emitted PAH and the N-PAHs degradation products, which are discussed in the next section.

Global PAH simulations are poorly constrained by available data, and many uncertainties exist in their emissions and atmospheric chemistry that affect the ability to model them accurately (see *Global Model Performance* in SI for more detail). A noted in Section 2.6, observations for Europe and North America were taken from continuously-monitoring air quality networks (EPA and EMEP) and those for continental Asia (Saha et al., 2017), Asia-Arctic ship cruise transect (Ma et al., 2013), and Africa (Klánová et al., 2008) are from field campaigns. Simulated and observed data at the location of measurements in Figure 1 are also represented in the form of box and whisker plots (Figure 2), where red reflects observed data, green reflects our base simulation, and blue shows a sensitivity simulation to test the influence of chemical uncertainties (described below). In Figure 2, PAH species on the x-axis are ordered from lowest molecular weight (left) to highest molecular weight (right). A summary of statistics are also shown in the SI (Table S1).

The model captures average PAH concentrations for most PAHs, but with some low biases, especially in urban areas. For 11 out of 16 emitted species, the p-value is less than 0.05 (indicated by * in Figure 2). Overall, simulated PAH concentrations are lower than observed (Figure 2B). For 13 of the emitted species, the model underpredicts the observed global average PAH concentration (normalized mean bias (NMB) ranges from -97 to -42 %; Figure 2B). For the remaining 3 emitted species (ACY, BKF and DAHA) the model overestimates the observed global-average PAH concentration (NMB = 104 to 464 %; Figure 2B). For non-urban sites (i.e. outside of cities), simulated PAH concentrations are lower than observed over the United States, and higher than observed over Europe. The bias over the US is likely a result of our choice of emission inventory: higher-resolution regional-scale emission inventories predict 2-3 times higher PAH emissions over the US (Zhang et al., 2017) compared to the global-scale emission inventory used in this study (Shen et al., 2013). Similar to other global-scale models (Friedman & Selin, 2012), our simulation underpredicts the high observed PAH concentrations typical of urban environments (Figure 1A-C; green circles), especially in cities across Asia and Africa. In remote regions, the model reproduces heavier molecular weight species measured across a ship cruise from Beijing (CH) to the Arctic (Ma et al., 2013), but underpredicts concentrations of lighter molecular weight species. In Svalbard (Norway), however, the model captures annual average PAH concentrations for the lighter molecular weight species, but underpredicts the

heavier molecular weight species by up to several orders of magnitude. Our model performance at capturing observed BAP concentrations is comparable to that of previous global-scale modelling studies (see discussion in the SI - *Global Model Performance*).

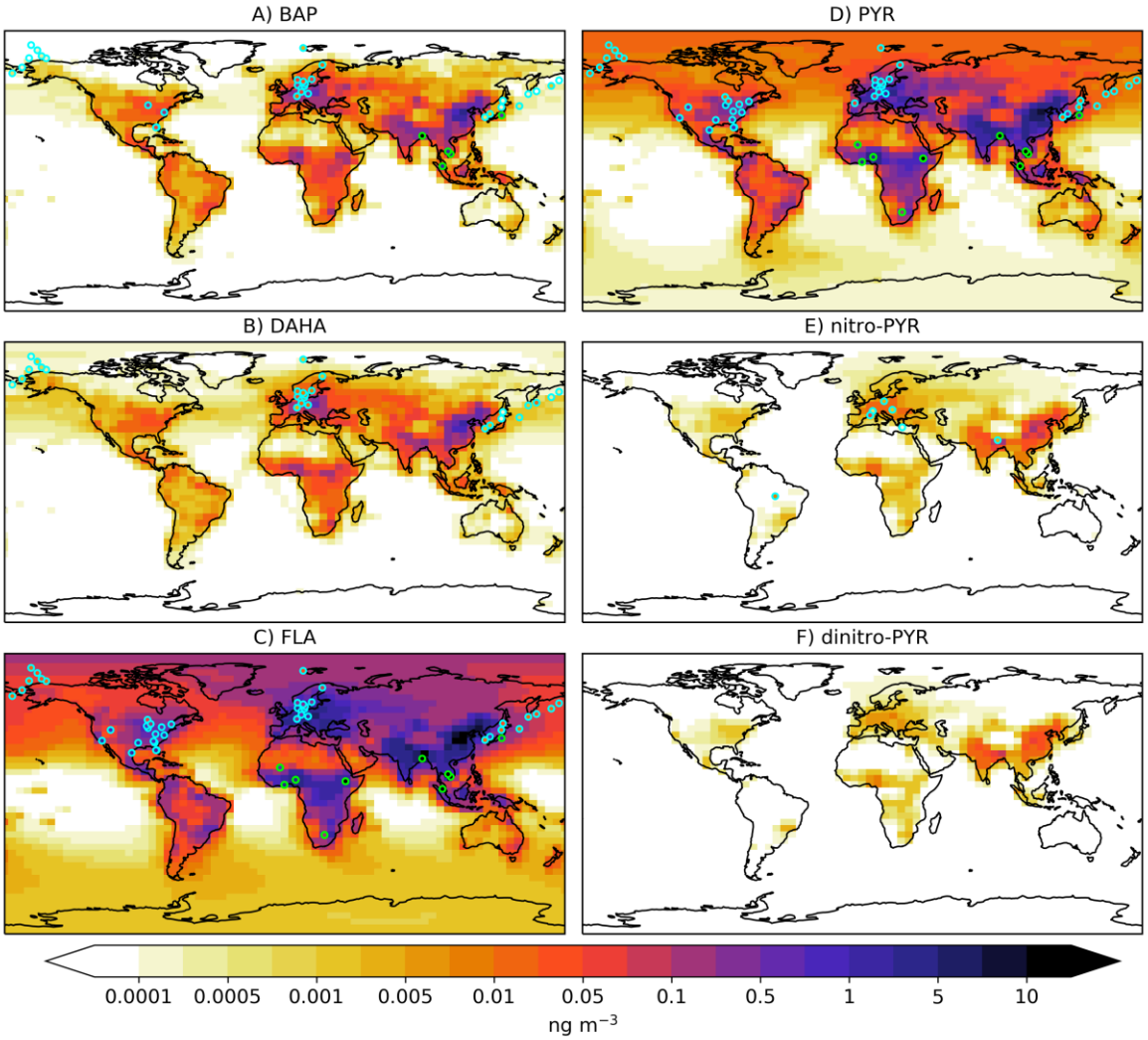

Figure 1. Spatial distributions of annual-average surface PAH concentrations (ng m^{-3}) in the GEOS-Chem model and overlaid with observed values. The left column shows three emitted PAHs: A) benzo[a]pyrene (BAP), B) dibenzo[a,h]anthracene (DAHA), and C) f fluoranthene (FLA). The right column shows a parent compound and its N-PAH degradation products: D) pyrene (PYR), E) nitropyrene (nitro-PYR), and F) dinitropyrene (dinitro-PYR). Circles represent observed concentrations. Green circles correspond to urban environments, and blue circles correspond to non-urban (background/remote) environments.

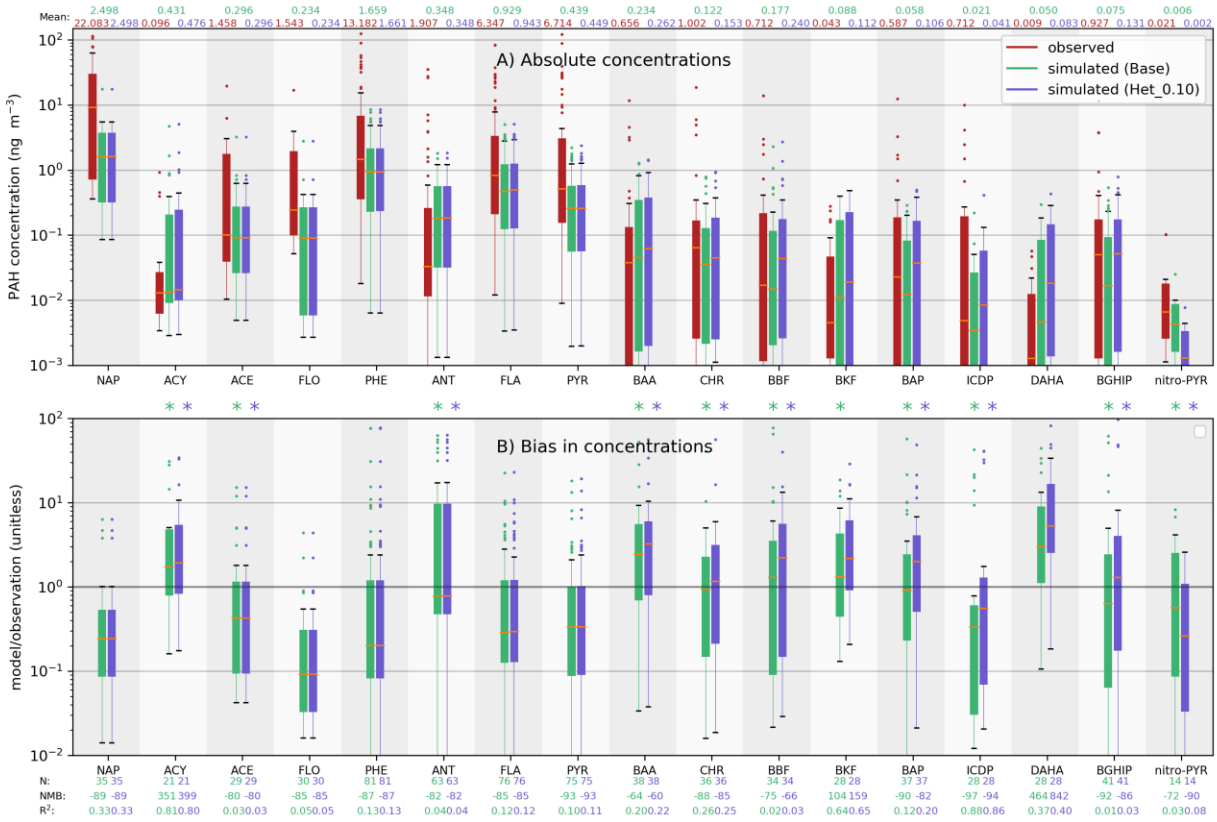

Figure 2. Box and whisker plot of PAH concentrations for all measurement sites displayed in Figure 1. Panel A shows concentrations (ng m^{-3}), with red representing the observed data, green representing the base model simulation, and blue representing simulated PAH concentrations under the sensitivity simulation (a 90 % reduction in the second order rate coefficients describing heterogeneous oxidation). The boxes denote the 25th and 75th percentiles, the whiskers denote the 5th and 95th percentiles, the horizontal line denotes the median, and dots denote outliers. Asterisks (*) indicate where p-value is less than 0.05. Panel B shows the ratio of simulated to observed PAH concentrations (unitless), with green representing the base, and blue representing the sensitivity simulation. The 16 directly emitted PAHs considered are naphthalene (NAP), acenaphthylene (ACY), acenaphthene (ACE), fluorene (FLO), phenanthrene (PHEN), anthracene (ANT), fluoranthene (FLA), pyrene (PYR), benzo[a]anthracene (BAA), chrysene (CHR), benzo[b]fluoranthene (BBF), benzo[k]fluoranthene (BKF), benzo[a]pyrene (BAP), benzo[g,h,i]perylene (BGHIP), indeno[1,2,3-c,d]pyrene (ICDP), and dibenz[a,h]anthracene (DAHA). Observations are described in greater detail in Materials and Methods, where full citations are provided.

We further evaluated model performance at capturing differences in concentrations between the different PAHs, both globally and in different regions, which are important to capture the relative cancer risk of different species (not shown). The lighter PAH species are much more abundant than the heavier species, both globally (Figure 2A) and regionally. The model generally captures these relative differences in PAH concentrations. Nevertheless, we

applied a simple "bias-correction" to the spatial distributions in PAH concentrations to test for the effects of a bias in the differences in concentrations across the different PAHs. Bias correction was conducted by multiplying the simulated PAH concentrations by the average bias between the simulated and observed mean PAH concentration across the non-urban sites (these bias-correction factors are shown in Table S1, SI). These bias-corrected PAH concentration distributions were used in the cancer risk assessment in a sensitivity calculation.

To test the ability of the model to simulate the atmospheric lifetime of different PAHs, which affects the composition of PAH mixtures when comparing source and receptor environments, we examined concentration gradients between Central Europe and the Arctic (Figure S1, SI). The model captures the observed PAH concentration gradient between Kocetice (Czech Republic) and Svalbard (Norway) for most of the lighter weight PAH species (ACY, ACE, PHE, ANT, FLA and PYR; Figure S1, SI). The model underpredicts this gradient for heavier PAHs (Figure S1, SI). While uncertainties in lifetimes and emissions combine to influence concentrations at remote sites (Thackray et al., 2015), these biases in lifetime are large enough to offset the likely overestimates in European emissions. To test the importance of these biases, we used the model sensitivity simulation that reduces the second order rate coefficient describing heterogeneous oxidation to 10 % of its original value ('Het_0.1'). Lighter PAHs are insensitive to changes in heterogeneous oxidation kinetics, as these species exist mostly in the gas-phase. The heavier molecular weight PAHs, which mostly exist in the particle-phase, are extremely sensitive to this sensitivity simulation. Under this simulation where heterogeneous oxidation kinetics are reduced to 10% of the value in the base simulation, the simulated PAH concentration gradients between Kocetice and Svalbard agree with observed values, and biases in PAH concentrations over Svalbard are minimized (Figure S1, SI). We use this sensitivity simulation below to test the influence of uncertainties in heterogeneous oxidation on estimates of human cancer risk (Figure 3 a).

For almost all continental regions, PAH concentrations are insensitive to uncertainties in gas-particle partitioning. The poly-parameter linear free energy relationship (ppLFER) gas-particle partitioning scheme used in the base model simulation captures observed particle fractions better than the D&E scheme used in the sensitivity simulation. While particle-phase fractions differed greatly between the two gas-particle partitioning schemes, annual-average PAH concentrations are within 5 % of each other over most continental environments under the two schemes. This is because of the very small differences between simulated gas- and particle-phase lifetimes.

3.2 Global and Regional Concentrations of PAH Degradation Products

We estimated the atmospheric concentrations of N-PAHs (nitro-PAHs and dinitro-PAHs) for all 16 of the emitted PAH discussed above (Section 2.4). Within the GEOS-Chem model, the chemical mechanism for pyrene (PYR) accounts for the formation of N-PYR (nitro-PYR and dinitro-PYR) (Table 1). Oxidative processes considered include gas-phase photooxidation (+OH) and direct nitration (+NO_3), and heterogeneous ozonolysis (+O_3) and direct nitration (+NO_3), all of which contribute to N-PYR formation, except heterogeneous ozonolysis. For the remaining N-PAHs, which are not incorporated into the online chemical mechanism, concentrations of the N-

PAHs were predicted offline by scaling concentrations of the remaining parent PAHs by spatially resolved ratios of nitro-PYR/PYR and dinitro-PYR/PYR (Figure S2, SI). This approach recognizes that detailed atmospheric degradation data for each individual PAH are not available, and thus provides a bounding estimate of the magnitude of N-PAH impacts under chemically-relevant background conditions. We used sensitivity calculations (described below) to further test the uncertainties introduced by this approach.

Simulated global mean atmospheric concentrations of nitro-PYR in the atmosphere are not statistically different from observations ($p<0.05$, Figure 2B). Spatial patterns in the N-PAHs (nitro-PYR and dinitro-PYR) and the parent PAH, PYR, are very similar (Figure 1D-F). Across non-urban sites, the model underpredicts the observed nitro-PYR concentration (0.016 ng m^{-3}) by a factor of 2.5. This bias is due to a combination of two factors. First, the model underestimates pyrene, the parent compound, by a factor of 1.4, likely due to underestimates of emissions, as described above. Second, our simulated nitro-PYR/PYR ratio of 0.021, is lower (x0.6) than the observed value (0.036) across the aggregated dataset of measurements, implying that we underestimate nitro-PAH formation on average. However, this is not consistent across all environments.

We compared the simulated N-PAH/PAH ratio to observed values from field campaigns, which measure the two species simultaneously (Table S2, SI). The simulated nitro-PYR/PYR ratio lies within the range of estimates from field campaigns; our value is x0.2, x0.7 and x3 times the value observed across China, France, Hungary, respectively. These biases vary across the different PAH species, but there were no systematic patterns (Table S2, SI). The simulated nitro-PAH/PAH ratios range from 2.0-4.0 fold of the observed ratios for FLA, 0.2-3.0 fold of the observed ratios for PYR, 0.06-10 fold of the observed ratios for CHR, and 0.02-5.0 fold of the observed ratios for BAP. To account for the impact of potential biases in estimating the cancer risk of PAHs and N-PAHs, we conducted sensitivity calculations by scaling the model-derived N-PAH/PAH ratio by the maximum/minimum bias between the simulated and observed N-PAH/PAH (these scaling factors are shown in Table S2, SI). This provides upper and lower bound estimates for N-PAH formation potential.

Heterogeneous direct nitration ($+NO_3$) is the major source of N-PAHs in the atmosphere, as discussed in greater detail in the SI (*Global and Regional Concentrations of PAH Degradation Products*). Globally, heterogeneous direct nitration accounts for 99 % of nitro-PYR production in the model. In laboratory studies, this process is a combination of multiple elementary reaction steps. Because the exact mechanism is unknown, we simulated it here using a single-step reaction. Laboratory studies find that the yield of N-PAHs from this process ranges 0.04 (Zelenov et al., 2018) – 100 (Ringuet et al., 2012) %. In our model, we assumed a fixed N-PAH formation yield, and chose 100 % in order to bound this reaction pathway; despite this maximal assumption, our model still underestimates the nitro-PYR/PYR ratio as discussed above.

The base simulation provides a better representation of the relative importance of parent PAHs and N-PAHs compared to the sensitivity simulation in which heterogeneous oxidation kinetics are reduced to 10 % of their laboratory values. PYR is insensitive to assumptions in heterogeneous oxidation kinetics, as this chemical reaction represents a minor removal term for this species compared with gas-phase oxidation. However, heterogeneous oxidation is the major

source of N-PAHs, so as this process slows down, concentrations of N-PAHs reduce. Reductions in the heterogeneous oxidation rate reduce the model's ability to capture the observed N-PYR concentration and N-PYR/PYR ratio (Figure 2B). Hence, while slower oxidation improves reaction kinetics for heavier molecular weight PAHs as discussed above, it decreases the model's ability to capture the observed concentration of N-PYR.

3.3 Human Cancer Risk of Ambient PAH Mixtures

We calculated the incremental lifetime cancer risk (ILCR) of PAHs (Figure 3) using two different methods (Section 2.6). Briefly, the epidemiologically-based method uses BAP as proxy for risk of the whole PAH mixture, the animal-based method accounts for regional variations in the PAH mixtures.

Using the animal-based method allowed us to compare the relative importance of different PAHs to ILCR (Figure 3A). BAP accounts for just 11 % of the calculated global human cancer risk of the entire pollutant mixture, with the remaining emitted PAHs accounting for 72 %, and the 12 N-PAHs (6 nitro-PAHs and 6 dinitro-PAHs) for which toxicity information is available account for the remaining 15 % of global ILCR (Figure 3A). The finding that BAP was of low importance to global human cancer risk (11 %) contradicts the findings of previous studies, but was robust across all sensitivity calculations conducted here (5 – 19 %; Figure 3A). Across our sensitivity calculations designed to capture the entire range of observed nitro-PAH/PAH ratios of the 6 PAHs considered, the contribution of N-PAHs to global ILCR ranges from 3-74 % (Figure 3 A). There are very few constraints on the nitro-PAH/PAH ratio; thus, we tested the limits of these values. While these sensitivity calculations gave some indication of the uncertainty related to the importance of N-PAHs, because each calculation used a single field study (i.e. single point) to constrain the entire global distribution of N-PAHs, they should be considered as extreme estimates for the importance of N-PAHs, and only applicable to environments close to where the field study is located. Despite these limitations, our model results suggest that N-PAHs could contribute substantially to global human health, even though they are routinely neglected in risk assessments.

Under the animal-based method, PAHs induce a global annual total human lung cancer rate of 231 $year^{-1}$, which is ~3 times lower than the rate estimated under the epidemiologically-based method (759 $year^{-1}$, Figure 3B). As noted above, epidemiologically-based methods implicitly address the impacts of mixtures of PAHs, because they are derived from studies in which people were exposed to multiple compounds simultaneously. Our animal-based method results in lower estimates because it includes only a small sample of all known PAHs – the 16 emitted species and the N-PAHs for which toxicity information is available. Our animal-based method also does not include other groups of PAHs which may be extremely toxic, such as oxygenated, halogenated and alkylated species (Andersson & Achten, 2015), and assumes that effects of individual PAHs add linearly. Thus, the overall magnitude of ILCR associated with PAHs is likely more realistic using the epidemiologically-based method. However, the epidemiologically-based method does not provide insight as to the toxicity and cancer risk of different chemical species and their respective degradation products. Further, the magnitude and spatial distribution of risk predicted by the epidemiologically-based method are only accurate to

the extent that global PAH concentrations reflect the mixtures to which people were exposed in the original epidemiological studies, and the degree that the overall risk scales with changes in BAP concentration. Under both methods for estimating ILCR, global ILCR exceeds the commonly-applied threshold level of 1 in 1,000,000 ($1x10^{-6}$); this is comparable in magnitude to estimates from previous studies (Figure 3A). Under the epidemiologically-based method for estimating human cancer risk of PAHs, 70 (63 - 82) % of the global population breathe air which exceeds this safe threshold level (with the ranging representing the upper and lower bounds in BAP toxicity).

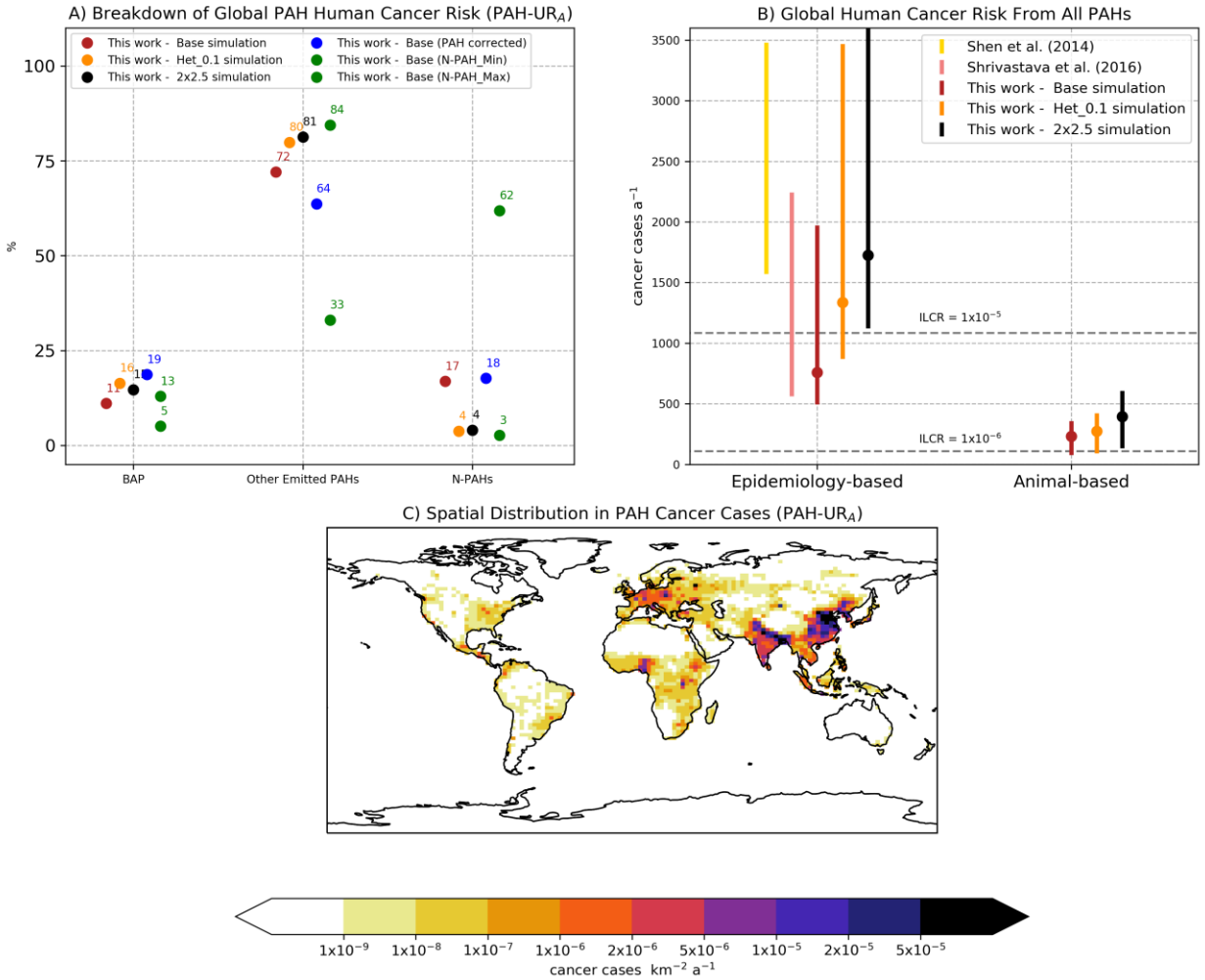

Figure 3. Global and regional impacts of ambient PAH concentrations on human cancer risk. Panel A shows a breakdown in global human cancer risk from different PAHs (%). Panel B shows global annual cancer rates (cancer cases a^{-1}) induced by PAHs, as estimated by two different methods (epidemiologically-based, and animal-based), and under three different model simulations (Base, Het_0.1, and 2x2.5). Estimates from the literature are also shown. Panel C shows the spatial pattern in PAH-induced human cancer rates under the base simulation, applying the animal-based method to estimate ILCR (but the pattern is similar for other formulations, which are not). Note that an ILCR of $1x10^{-6}$, applied to the global population

564 (~$7x10^9$) is equal to $7x10^3$ lifetime cancer cases, and assuming a life expectancy of 70 years,
565 equates to an annual cancer rate of 100.

566 Under the animal-based method, human cancer risk is much less sensitive to uncertainties
567 in PAH heterogeneous oxidation kinetics than that reported in previous studies using BAP as an
568 indicator species (Shrivastava et al., 2017). This is because when particle-phase PAHs are
569 assumed to be less reactive, concentrations of the parent compounds increase, while
570 concentrations of the oxidation products decrease. Previous studies, which have used the
571 epidemiologically-based method, only accounted for the former (increased human exposure to
572 the parent compound), whereas the animal-based method used here also accounts for the latter
573 (decreased concentrations of the degradation products). Compared to the base simulation (Base =
574 0.19 ng m^{-3}), the global-average population-weighted BAP concentration is 90 % higher in the
575 sensitivity simulation that tests the impact of oxidation kinetics (Het_0.1 = 0.36 ng m^{-3}). Under
576 the epidemiology-based method for estimating ILCR, where the cancer risk of PAHs scale
577 closely with BAP, global ILCR is 76 % higher in the sensitivity simulation (1335 $year^{-1}$)
578 compared to the standard version of the model (759 $year^{-1}$). However, the animal-based method
579 shows a much weaker sensitivity in global ILCR to particle-phase reactivity. For the same
580 increase in BAP exposure (+ 90 %), the global ILCR increases by only 18 %, from 231 to 273
581 $year^{-1}$ (Figure 3B). Under this method, while slower particle-phase reactivity increases human
582 exposure to the parent compounds, this is partially offset by reductions in exposure to the
583 oxidation products. The animal-based method thus provides a more realistic estimate of the
584 impact of heterogeneous oxidation uncertainty on cancer risks. Human cancer risk is also
585 insensitive to uncertainties in gas-particle partitioning. Both globally and regionally, the ILCR
586 changes by less than 1 % when the gas-particle partitioning scheme is changed from the ppLFER
587 scheme used in the base model simulation, to the D&E scheme used in the sensitivity simulation.
588 Similarly, when the model resolution is increased from 4° x 5° in the base simulation to 2° x 2.5°
589 in a sensitivity simulation ('2x2.5'), global ILCR increases by 29 % - however, the relative
590 importance of each PAH species to global ILCR remains unchanged.

591 Although omitted from previous global-scale assessments, uncertainties in BAP toxicity
592 also play a substantial role in influencing the magnitude in global ILCR from PAHs. In Figure
593 3B, for our estimates of global ILCR, the length of the bars represent the uncertainty bounds in
594 BAP toxicity, but for Shen et al. (2014) and Shrivastava et al. (2017), they represent
595 uncertainties associated with genetic susceptibility and heterogeneous oxidation kinetics,
596 respectively. From Figure 3B, under the epidemiologically-based method, uncertainties
597 associated with BAP toxicity (length of red and orange bars in Figure 3B have a larger influence
598 on global ILCR than uncertainties in genetic susceptibility (lengths of yellow colored bar in
599 Figure 3B) and uncertainties in heterogeneous oxidation kinetics (length of peach colored bar in
600 Figure 3B), highlighting the importance of future research on this parameter.

601 Under the epidemiologically-based and animal-based methods, human cancer risk
602 associated with PAHs is highest in urban and industrial regions, but the two methods differ in
603 their assessments of the spatial variability of these risks. Both methods predict PAH exposure
604 leads to the highest human cancer risk over regions such as China, India, Central and Eastern
605 Europe (Figure 3C). Under the epidemiologically-based method, however, differences in ILCR
606 are driven solely by BAP, whereas under the animal-based method, the ILCR varies spatially
607 with BAP and many other PAHs. When assessing the impact on human cancer risk of reducing

BAP emissions (not shown), the epidemiologically-based method would estimate a proportional reduction in the human cancer risk, but the animal-based method would estimate a reduction in human cancer risk a factor of three or more lower (which would vary based on the regional variations in the contribution of BAP to total ILCR).

5 Conclusions

We developed and evaluated a new, global-scale model that accounts for 16 emitted PAHs in addition to their degradation products. We used this model to calculate the human cancer risk of exposure to these PAH mixtures using two different methods: an epidemiologically-based method based on BAP concentrations that quantifies overall risk, and an animal-based method that allowed us to attribute risk to individual components of the pollutant mixture without double counting. We then evaluated the relative importance of BAP to global risk, and assessed the utility of using BAP as an indicator compound.

We found that BAP is only a small contributor to the global human cancer risk of PAHs (11 %), suggesting it is an inadequate indicator of human cancer risk from this pollutant mixture. Atmospheric modeling studies typically only consider a single PAH species (BAP), and our work suggests that conclusions based on modeling this single compound can be misleading or erroneous. In previous studies, BAP accounted for 40 to 80 % of the cancer risk of PAHs (Delgado-Saborit et al., 2011; Nielsen et al., 1996; Norramit et al., 2005; Zhang et al., 2016; Zhang et al., 2009). However, Zhang et al. (2016) only considered 8 PAHs, which partially explain their high BAP contribution to ILCR over the US (9-154 a^{-1}) of 40-60 %. In our study, where we considered 16 emitted PAHs and 12 N-PAHs, BAP accounted for 6-15 % of ILCR over the same region. The assumed toxicity of DAHA (ranging from 1-10 times that of BAP), and whether it is even included, varies from study to study. Nielsen et al. (1996), who estimated that BAP accounts for 70% of cancer risk in a field study, did not include DAHA in their analysis. In addition, several highly toxic PAHs were not included in this study, due to lack of data to constrain their emissions and chemistry. Anderson et al. (2015) argues that, in addition to the USEPA16 and N-PAHs, scientific research should be expanded further still, to include other highly toxic parent PAHs and degradation products with an oxy group (O-PAHs). However, atmospheric emission inventories are available only for the USEPA16, and current understanding of O-PAHs is insufficient to build chemical mechanisms within atmospheric models. However, including further PAHs and degradation products would almost certainly further diminish the importance of BAP, strengthening our main conclusions.

In addition to the emitted PAHs, we also considered N-PAHs, and we found them to be an important contributor to human cancer risk, but unlike BAP and the other USEPA16, they are not regulated or routinely monitored. Previous assessments of the impact of N-PAHs were limited to a small number of field campaigns and a single box-model study. Our model simulations showed that wherever PAHs are emitted, there is sufficient NO_3 to allow the formation of N-PAHs. Accounting for 15-20 % of the carcinogenic potential of PAH mixtures, we estimated that N-PAHs are comparably dangerous for human cancer risk to BAP (11%). In our sensitivity calculations, the uncertainty in N-PAH/PAH concentration ratios led to considerable variance in the contribution of N-PAH to human cancer risk. Increased confidence

in this class of chemical would be provided by (i) a deeper understanding of the formation processes (yields and mechanisms), (ii) a wider understanding of the toxicity of N-PAHs, and (iii) greater geographical coverage and density of observations. Furthermore, in addition to being formed during the oxidation of parent PAHs, as simulated here, N-PAHs can also be directly emitted into the atmosphere. We do not consider direct emissions of N-PAHs in our atmospheric model. Our simulations, however, are constrained by observed values of N-PAHs, thus we believe our result that N-PAHs contribute 15-20 % to global ILCR is a robust bounding estimate. Nevertheless, providing better constraints on the source of N-PAHs in the atmosphere should be a future research priority, especially if mitigation measures are to be considered.

PAHs and their degradation products, including N-PAHs, can have a complex impact on human cells, altering transcriptional profiles, signaling networks, and in many cases causing DNA adducts that eventually can progress to DNA mutations. While most research has been focused on understanding the response of cells to single PAH species such as BAP, cancer risk data highlight the need to consider more complex, real-world mixtures of PAHs in order to better define the interactions between different compounds and develop more accurate predictive models.

PAHs pose a substantial threat to global human cancer risk across all of our simulations and the two methods for estimating ILCR. We estimated an overall annual cancer risk of 231-759 $year^{-1}$ from ambient exposure to PAHs globally. Across each of the model simulations and methods in this study, as well as in previous studies, global ILCR exceeded the commonly-applied threshold level of 1 in 1,000,000 ($1x10^{-6}$) (Figure 3B). Our epidemiologically-based estimate using our base simulation nevertheless calculated a lower global cancer risk than previous studies. Results from Shen et al. (2014) and Shrivastava et al. (2017) are shown for comparison in Figure 3B. Our estimates were lower for three reasons. First, Shen et al. (2014) and Shrivastava et al. (2017) choose to "downscale" their simulated BAP concentrations to reduce bias in urban environments, whereas we did not. Downscaling introduces additional uncertain parameters; we chose instead to apply the best available physical, process-based and explore the importance of simulation biases more directly through supplementary calculations. Second, we used median estimates of the toxicity of BAP, whereas Shen et al. (2014) and Shrivastava et al. (2017) used maximum estimates from the literature. Third, to facilitate comparison of the variability driven by the concentration of different PAHs, we did not account for variability in cancer susceptibility in either of our methods for estimating ILCR, which has been shown to double global ILCR.

Our animal-based method provides a more realistic description for spatial differences in the human cancer risk associated with PAHs, as it captures regional differences in PAH mixtures. For example, simulated annual-average BAP concentrations were 3.5 times higher over Hong Kong compared to southern India. Using the epidemiologically-based method, the calculated difference in ILCR between these two locations also differed by the same amount (x3.5), but the animal-based method suggested that cancer risk in Hong Kong is 12 times higher than over southern India. Hong Kong had a particularly high contribution of DAHA, which the epidemiologically-based method did not account for. This suggests that variations in BAP should not be viewed as indicators of variation in human cancer risk due to PAH mixtures, which is a common conclusion drawn from atmospheric models of BAP alone.

While toxicity information used in the animal-based method may not be exactly representative of humans, it does allow us to compare the individual risk of different species in the PAH mixture. PAHs impart their toxic effects on cells through complex pathways that include responses to DNA damage and protein-mediated cellular signaling pathways that alter gene expression of several cytochrome P450s and other enzymes. The expression of PAH-responsive enzymes can vary widely between animals and humans, resulting in differences in susceptibility to these compounds. However, in this study we used literature values of the relative toxicities of PAHs compared to BAP, where mechanisms of action for different PAH species are often similar between animals and humans. There are no human data on the relative toxicities of these PAHs, making us reliant on toxicity data derived from animals where multiple different PAHs have been tested individually in animals. Mechanisms for differences in relative toxicities of PAHs and their nitro derivatives are not yet well understood; however, in most cases, the differences have been attributed to differences in absorption, transport and solubility of compounds in the body (Fu, 1990). More comprehensive understanding of how these pharmacokinetic parameters differ between animal and humans and among different PAH species could further extend the applicability of our animal-based method.

In contrast to previous studies, we found that the cancer risks associated with PAHs are not sensitive to uncertainties in heterogeneous oxidation kinetics. As discussed above, when particle-phase PAHs were assumed to be less reactive, concentrations of the parent compounds increase at the expense of concentrations of the oxidation products. Hence, in the animal-based method for estimating human cancer risk, where both emitted PAHs and the degradation products are considered, global ILCR increased by 18 %. Contrastingly, in the epidemiologically-based method for estimating ILCR, which only considers concentrations of a single parent compound (BAP), global ILCR increased by 76 %. This reduced sensitivity contradicts previous results by Shrivastava et al. (2017), who estimated, using an epidemiologically-based method, that reductions in reactivity (due to a hypothesized mechanism including particle shielding) increased global ILCR by a factor of 4, corresponding with five-fold estimates of global-average population-weighted BAP concentration. Hence, our holistic view of PAHs, considering both parent compounds and oxidative derivatives, weakens the sensitivity of PAH human cancer risk to uncertainties in heterogeneous oxidation kinetics. In addition, the human cancer risk associated with PAHs was insensitive to uncertainties in gas-particle partitioning. When then the gas-particle partitioning scheme was changed from the ppLFER to the D&E scheme, global cancer risk changed by less than 1 %.

Overall, we conclude that BAP is a poor indicator of human health risks, and that other emitted PAHs and N-PAHs are the dominant contributors to the human cancer risk of PAHs. Researchers and governing bodies should consider extending assessment and monitoring beyond BAP in order to better capture who is affected, and how the health impacts could be mitigated. Increased observations, especially outside North America and Europe, are needed to provide stronger constraints on human exposure to PAHs. We have shown that N-PAHs, which account for only ~1 % of the oxidation products, contribute to human cancer risk. Future research is required to quantify the human health impacts of the remaining PAH degradation products, which will involve a deeper understanding of the chemical mechanisms and kinetics, and the products' toxicity.

Acknowledgments, Samples, and Data

The authors declare no financial conflicts of interests. All data associated with this research is publicly available. A data directory containing the GEOS-Chem model code, as well as the python scripts to analysis this code, will be made available in a public repository (likely Zenodo) upon publication of the peer-reviewed manuscript. We thank John M. Essigmann, Robert Croy, and Bogdan Fedeles for providing historical context for the toxicological importance of BAP. We also thank Sebastian D. Eastham for his continued support in running the GEOS-Chem model. We acknowledge the National Institute of Environmental Health Sciences Superfund Basic Research Program, National Institute of Health, P42 ES027707, and the MIT Center for Precision Cancer Medicine. This work was also supported by the University of York's Viking research computing facility.

References

Albinet, A., Leoz-Garziandia, E., Budzinski, H., & ViIlenave, E. (2007). Polycyclic aromatic hydrocarbons (PAHs), nitrated PAHs and oxygenated PAHs in ambient air of the Marseilles area (South of France): Concentrations and sources. *Science of the Total Environment, 384*(1-3), 280-292. doi:10.1016/j.scitotenv.2007.04.028

Amos, H. M., Jacob, D. J., Holmes, C. D., Fisher, J. A., Wang, Q., Yantosca, R. M., . . . Sunderland, E. M. (2012). Gas-particle partitioning of atmospheric Hg(II) and its effect on global mercury deposition. *Atmospheric Chemistry and Physics, 12*(1), 591-603. doi:10.5194/acp-12-591-2012

Andersson, J. T., & Achten, C. (2015). Time to Say Goodbye to the 16 EPA PAHs? Toward an Up-to-Date Use of PACs for Environmental Purposes. *Polycyclic Aromatic Compounds, 35*(2-4), 330-354. doi:10.1080/10406638.2014.991042

Armstrong, B., Hutchinson, E., Unwin, J., & Fletcher, T. (2004). Lung cancer risk after exposure to polycyclic aromatic hydrocarbons: A review and meta-analysis. *Environmental Health Perspectives, 112*(9), 970-978. doi:10.1289/ehp.6895

Atkinson, R., Arey, J., Zielinska, B., & Aschmann, S. M. (1990). Kinetics and nitro-products of the gas-phase oh and NO_3 radical-initiated reactions of naphthalene-d8, fluoranthene-d10, and pyrene. *International Journal of Chemical Kinetics, 22*(9), 999-1014. doi:10.1002/kin.550220910

Bey, I., Jacob, D. J., Yantosca, R. M., Logan, J. A., Field, B. D., Fiore, A. M., . . . Schultz, M. G. (2001). Global modeling of tropospheric chemistry with assimilated meteorology: Model description and evaluation. *Journal of Geophysical Research-Atmospheres, 106*(D19), 23073-23095. doi:10.1029/2001jd000807

Bostrom, C. E., Gerde, P., Hanberg, A., Jernstrom, B., Johansson, C., Kyrklund, T., . . . Westerholm, R. (2002). Cancer risk assessment, indicators, and guidelines for polycyclic aromatic hydrocarbons in the ambient air. *Environmental Health Perspectives, 110*, 451-488. doi:10.1289/ehp.02110s3451

Busby, W. F., Stevens, E. K., Martin, C. N., Chow, F. L., & Garner, R. C. (1989). Comparative lung tumorigenicity of parent and mononitro-polynuclear aromatic-hydrocarbons in the BLU:Ha newborn mouse assay. *Toxicology and Applied Pharmacology, 99*(3), 555-563. doi:10.1016/0041-008x(89)90162-2

781 Collins, J. F., Brown, J. P., Dawson, S. V., & Marty, M. A. (1991). Risk assessment for benzo[a]
782 pyrene. *Regulatory Toxicology and Pharmacology, 13*(2), 170-184. doi:10.1016/0273-
783 2300(91)90020-v
784 Crippa, M., Guizzardi, D., Muntean, M., Schaaf, E., Dentener, F., van Aardenne, J. A., . . .
785 Janssens-Maenhout, G. (2018). Gridded emissions of air pollutants for the period 1970-
786 2012 within EDGAR v4.3.2. *Earth System Science Data, 10*(4), 1987-2013.
787 doi:10.5194/essd-10-1987-2018
788 Dachs, J., & Eisenreich, S. J. (2000). Adsorption onto aerosol soot carbon dominates gas-particle
789 partitioning of polycyclic aromatic hydrocarbons. *Environmental Science & Technology,*
790 *34*(17), 3690-3697. doi:10.1021/es991201+
791 Delgado-Saborit, J. M., Stark, C., & Harrison, R. M. (2011). Carcinogenic potential, levels and
792 sources of polycyclic aromatic hydrocarbon mixtures in indoor and outdoor environments
793 and their implications for air quality standards. *Environment International, 37*(2), 383-
794 392. doi:10.1016/j.envint.2010.10.011
795 Deutschwenzel, R. P., Brune, H., Grimmer, G., Dettbarn, G., & Misfeld, J. (1983). Experimental
796 studies in rat lungs on the carcinogenicity and dose-response relationships of 8 frequently
797 occurring environmental polycyclic aromatic-hydrocarbons. *Jnci-Journal of the National*
798 *Cancer Institute, 71*(3), 539-544.
799 Dixon, H. M., Armstrong, G., Barton, M., Bergmann, A. J., Bondy, M., Halbleib, M. L., . . .
800 Anderson, K. A. (2019). Discovery of common chemical exposures across three
801 continents using silicone wristbands. *Royal Society Open Science, 6*(2), 19.
802 doi:10.1098/rsos.181836
803 Drotikova, T., Ali, A. M., Halse, A. K., Reinardy, H. C., & Kallenborn, R. (2020). Polycyclic
804 aromatic hydrocarbons (PAHs) and oxy- and nitro-PAHs in ambient air of the Arctic
805 town Longyearbyen, Svalbard. *Atmospheric Chemistry and Physics, 20*(16), 9997-10014.
806 doi:10.5194/acp-20-9997-2020
807 Eastham, S. D., Weisenstein, D. K., & Barrett, S. R. H. (2014). Development and evaluation of
808 the unified tropospheric-stratospheric chemistry extension (UCX) for the global
809 chemistry-transport model GEOS-Chem. *Atmospheric Environment, 89*, 52-63.
810 doi:10.1016/j.atmosenv.2014.02.001
811 Elzein, A., Dunmore, R. E., Ward, M. W., Hamilton, J. F., & Lewis, A. C. (2019). Variability of
812 polycyclic aromatic hydrocarbons and their oxidative derivatives in wintertime Beijing,
813 China. *Atmospheric Chemistry and Physics, 19*(13), 8741-8758. doi:10.5194/acp-19-
814 8741-2019
815 Environmental Protection Agency Air Toxics, https://www.epa.gov/haps (accessed on
816 September 23, 2020).
817 United States Environmental Protection Agency (2009). *Development of a Relative Potency*
818 *Factor (RPF) Approach for Polycyclic Aromatic Hydrocarbon (PAH) Mxitures*
819 *(Interagency Science Consultation Draft)*. Retrieved from
820 https://cfpub.epa.gov/si/si_public_record_report.cfm?Lab=NCEA&dirEntryId=194584
821 (accessed on September 23, 2020).
822 European Monitoring and Evaluation Programme (EMEP). Retrieved from https://www.emep.int
823 (accessed on September 23, 2020).
824 Feilberg, A., Kamens, R. M., Strommen, M. R., & Nielsen, T. (1999). Modeling the formation,
825 decay, and partitioning of semivolatile nitro-polycyclic aromatic hydrocarbons

(nitronaphthalenes) in the atmosphere. *Atmospheric Environment, 33*(8), 1231-1243. doi:10.1016/s1352-2310(98)00275-1

Fountoukis, C., & Nenes, A. (2007). ISORROPIA II: a computationally efficient thermodynamic equilibrium model for K^+-Ca^{2+}-Mg^{2+}-$NH_{(4)}^{(+)}$-Na^+-SO_4^{2-}-NO_3^--Cl^--H_2O aerosols. *Atmospheric Chemistry and Physics, 7*(17), 4639-4659. doi:10.5194/acp-7-4639-2007

Friedman, C. L., Pierce, J. R., & Selin, N. E. (2014). Assessing the Influence of Secondary Organic versus Primary Carbonaceous Aerosols on Long-Range Atmospheric Polycyclic Aromatic Hydrocarbon Transport. *Environmental Science & Technology, 48*(6), 3293-3302. doi:10.1021/es405219r

Friedman, C. L., & Selin, N. E. (2012). Long-Range Atmospheric Transport of Polycyclic Aromatic Hydrocarbons: A Global 3-D Model Analysis Including Evaluation of Arctic Sources. *Environmental Science & Technology, 46*(17), 9501-9510. doi:10.1021/es301904d

Friedman, C. L., Zhang, Y. X., & Selin, N. E. (2014). Climate Change and Emissions Impacts on Atmospheric PAH Transport to the Arctic. *Environmental Science & Technology, 48*(1), 429-437. doi:10.1021/es403098w

Fu, P. P. (1990). Metabolism of nitro-polycyclic aromatic-hydrocarbons. *Drug Metabolism Reviews, 22*(2-3), 209-268. doi:10.3109/03602539009041085

Fu, P. P., Von Tungeln, L. S., Chiu, L. H., Zhan, D. J., Deck, J., Bucci, T., & Wang, J. C. (1998). Structure, tumorigenicity, microsomal metabolism, and DNA binding of 7-nitrodibenz a,h anthracene. *Chemical Research in Toxicology, 11*(8), 937-945. doi:10.1021/tx980079+

GEOS-Chem (wiki page). Retrieved from http://wiki.seas.harvard.edu/geos-chem/index.php/Main_Page (accessed on September 23, 2020).

Giglio, L., Randerson, J. T., & van der Werf, G. R. (2013). Analysis of daily, monthly, and annual burned area using the fourth-generation global fire emissions database (GFED4). *Journal of Geophysical Research-Biogeosciences, 118*(1), 317-328. doi:10.1002/jgrg.20042

Modern-Era Retrospective analysis for Research and Applications Version 2, Global Modeling and Assimilation Office The Modern-Era Retrospective analysis for Research and Applications (Version 2). Retrieved from https://gmao.gsfc.nasa.gov/reanalysis/MERRA-2/ (accessed on September 23, 2020).

Gray, J. S. (2002). Biomagnification in marine systems: the perspective of an ecologist. *Marine Pollution Bulletin, 45*(1-12), 46-52. doi:10.1016/s0025-326x(01)00323-x

Guenther, A. B., Jiang, X., Heald, C. L., Sakulyanontvittaya, T., Duhl, T., Emmons, L. K., & Wang, X. (2012). The Model of Emissions of Gases and Aerosols from Nature version 2.1 (MEGAN2.1): an extended and updated framework for modeling biogenic emissions. *Geoscientific Model Development, 5*(6), 1471-1492. doi:10.5194/gmd-5-1471-2012

Hansen, T., Seidel, A., & Borlak, J. (2007). The environmental carcinogen 3-nitrobenzanthrone and its main metabolite 3-aminobenzanthrone enhance formation of reactive oxygen intermediates in human A549 lung epithelial cells. *Toxicology and Applied Pharmacology, 221*(2), 222-234. doi:10.1016/j.taap.2007.03.003

Heinrich, U., Roller, M., & Pott, F. (1994). Estimation of a lifetime unit lung-cancer risk for benzo(a)pyrene based on tumor rates in rats exposed to coal tar/pitch condensation aerosol. *Toxicology Letters, 72*(1-3), 155-161. doi:10.1016/0378-4274(94)90023-x

Hu, L., Millet, D. B., Baasandorj, M., Griffis, T. J., Travis, K. R., Tessum, C. W., . . . de Gouw, J. (2015). Emissions of C-6-C-8 aromatic compounds in the United States: Constraints from tall tower and aircraft measurements. *Journal of Geophysical Research-Atmospheres, 120*(2), 826-842. doi:10.1002/2014jd022627

Keyte, I. J., Harrison, R. M., & Lammel, G. (2013). Chemical reactivity and long-range transport potential of polycyclic aromatic hydrocarbons - a review. *Chemical Society Reviews, 42*(24), 9333-9391. doi:10.1039/c3cs60147a

Klánová, J., Cupr, P., Holoubek, I., Boruvková, J., Pˇribylová, P., Kareš, R., . . . Ocelka, T. (2008). *Application of passive sampler for monitoring of POPs in ambient air. VI. Pilot study for development of the monitoring network in the African continent (MONET-AFRICA 2008).* (Doctoral thesis). Retrieved from author. Location: Masaryk University,

Koch, R., Knispel, R., Elend, M., Siese, M., & Zetzsch, C. (2007). Consecutive reactions of aromatic-OH adducts with NO, NO_2 and O_2: benzene, naphthalene, toluene, m- and p-xylene, hexamethylbenzene, phenol, m-cresol and aniline. *Atmospheric Chemistry and Physics, 7*(8), 2057-2071. doi:10.5194/acp-7-2057-2007

Lammel, G., Mulder, M. D., Shahpoury, P., Kukucka, P., Liskova, H., Pribylova, P., . . . Wotawa, G. (2017). Nitro-polycyclic aromatic hydrocarbons - gas-particle partitioning, mass size distribution, and formation along transport in marine and continental background air. *Atmospheric Chemistry and Physics, 17*(10), 6257-6270. doi:10.5194/acp-17-6257-2017

Lammel, G., Sehili, A. M., Bond, T. C., Feichter, J., & Grassl, H. (2009). Gas/particle partitioning and global distribution of polycyclic aromatic hydrocarbons - A modelling approach. *Chemosphere, 76*(1), 98-106. doi:10.1016/j.chemosphere.2009.02.017

Liu, C. G., Zhang, P., Yang, B., Wang, Y. F., & Shu, J. N. (2012). Kinetic Studies of Heterogeneous Reactions of Polycyclic Aromatic Hydrocarbon Aerosols with NO_3 Radicals. *Environmental Science & Technology, 46*(14), 7575-7580. doi:10.1021/es301403d

Ma, Y. X., Xie, Z. Y., Yang, H. Z., Moller, A., Halsall, C., Cai, M. H., . . . Ebinghaus, R. (2013). Deposition of polycyclic aromatic hydrocarbons in the North Pacific and the Arctic. *Journal of Geophysical Research-Atmospheres, 118*(11), 5822-5829. doi:10.1002/jgrd.50473

Miet, K., Le Menach, K., Flaud, P. M., Budzinski, H., & Villenave, E. (2009). Heterogeneous reactions of ozone with pyrene, 1-hydroxypyrene and 1-nitropyrene adsorbed on particles. *Atmospheric Environment, 43*(24), 3699-3707. doi:10.1016/j.atmosenv.2009.04.032

Moolgavkar, S. H., Luebeck, E. G., & Anderson, E. L. (1998). Estimation of unit risk for coke oven emissions. *Risk Analysis, 18*(6), 813-825. doi:10.1111/j.1539-6924.1998.tb01124.x

Mu, Q., Shiraiwa, M., Octaviani, M., Ma, N., Ding, A. J., Su, H., . . . Cheng, Y. F. (2018). Temperature effect on phase state and reactivity controls atmospheric multiphase chemistry and transport of PAHs. *Science Advances, 4*(3). doi:10.1126/sciadv.aap7314

Mulder, M. D., Dumanoglu, Y., Efstathiou, C., Kukucka, P., Matejovicova, J., Maurer, C., . . . Lammel, G. (2019). Fast Formation of Nitro-PAHs in the Marine Atmosphere Constrained in a Regional-Scale Lagrangian Field Experiment. *Environmental Science & Technology, 53*(15), 8914-8924. doi:10.1021/acs.est.9b03090

Nielsen, T., Jorgensen, H. E., Larsen, J. C., & Poulsen, M. (1996). City air pollution of polycyclic aromatic hydrocarbons and other mutagens: Occurrence, sources and health

effects. *Science of the Total Environment, 189*, 41-49. doi:10.1016/0048-9697(96)05189-3

Nisbet, I. C. T., & Lagoy, P. K. (1992). Toxic equivalency factors (TEFs) for polycyclic aromatic-hydrocarbons (PAHS). *Regulatory Toxicology and Pharmacology, 16*(3), 290-300. doi:10.1016/0273-2300(92)90009-x

Norramit, P., Cheevaporn, V., Itoh, N., & Tanaka, K. (2005). Characterization and carcinogenic risk assessment of polycyclic aromatic hydrocarbons in the respirable fraction of airborne particles in the Bangkok Metropolitan area. *Journal of Health Science, 51*(4), 437-446. doi:10.1248/jhs.51.437

Norwegian Institute for Air Research. Retrieved from http://ebas.nilu.no (accessed on September 23, 2020).

Octayiani, M., Tost, H., & Lammel, G. (2019). Global simulation of semivolatile organic compounds - development and evaluation of the MESSy submodel SVOC (v1.0). *Geoscientific Model Development, 12*(8), 3585-3607. doi:10.5194/gmd-12-3585-2019

Park, E. J., & Park, K. (2009). Induction of pro-inflammatory signals by 1-nitropyrene in cultured BEAS-2B cells. *Toxicology Letters, 184*(2), 126-133. doi:10.1016/j.toxlet.2008.10.028

Perraudin, E., Budzinski, H., & Villenave, E. (2007). Kinetic study of the reactions of ozone with polycyclic aromatic hydrocarbons adsorbed on atmospheric model particles. *Journal of Atmospheric Chemistry, 56*(1), 57-82. doi:10.1007/s10874-006-9042-x

Poschl, U., Letzel, T., Schauer, C., & Niessner, R. (2001). Interaction of ozone and water vapor with spark discharge soot aerosol particles coated with benzo a pyrene: O_3 and H_2O adsorption, benzo a pyrene degradation, and atmospheric implications. *Journal of Physical Chemistry A, 105*(16), 4029-4041. doi:10.1021/jp004137n

Ringuet, J., Albinet, A., Leoz-Garziandia, E., Budzinski, H., & Villenave, E. (2012). Reactivity of polycyclic aromatic compounds (PAHs, NPAHs and OPAHs) adsorbed on natural aerosol particles exposed to atmospheric oxidants. *Atmospheric Environment, 61*, 15-22. doi:10.1016/j.atmosenv.2012.07.025

Saha, M., Maharana, D., Kurumisawa, R., Takada, H., Yeo, B. G., Rodrigues, A. C., . . . Viet, P. H. (2017). Seasonal Trends of Atmospheric PAHs in Five Asian Megacities and Source Detection Using Suitable Biomarkers. *Aerosol and Air Quality Research, 17*(9), 2247-2262. doi:10.4209/aaqr.2017.05.0163

Sander, R. (2015). Compilation of Henry's law constants (version 4.0) for water as solvent. *Atmospheric Chemistry and Physics, 15*(8), 4399-4981. doi:10.5194/acp-15-4399-2015

Shahpoury, P., Lammel, G., Albinet, A., Sofuoglu, A., Dumanoglu, Y., Sofuoglu, S. C., . . . Zdimal, V. (2016). Evaluation of a Conceptual Model for Gas-Particle Partitioning of Polycyclic Aromatic Hydrocarbons Using Polyparameter Linear Free Energy Relationships. *Environmental Science & Technology, 50*(22), 12312-12319. doi:10.1021/acs.est.6b02158

Shen, H. Z., Huang, Y., Wang, R., Zhu, D., Li, W., Shen, G. F., . . . Tao, S. (2013). Global Atmospheric Emissions of Polycyclic Aromatic Hydrocarbons from 1960 to 2008 and Future Predictions. *Environmental Science & Technology, 47*(12), 6415-6424. doi:10.1021/es400857z

Shen, H. Z., Tao, S., Liu, J. F., Huang, Y., Chen, H., Li, W., . . . Liu, W. X. (2014). Global lung cancer risk from PAH exposure highly depends on emission sources and individual susceptibility. *Scientific Reports, 4*. doi:10.1038/srep06561

963 Shrivastava, M., Lou, S., Zelenyuk, A., Easter, R. C., Corley, R. A., Thrall, B. D., . . . Tao, S.
964 (2017). Global long-range transport and lung cancer risk from polycyclic aromatic
965 hydrocarbons shielded by coatings of organic aerosol. *Proceedings of the National*
966 *Academy of Sciences of the United States of America*, *114*(6), 1246-1251.
967 doi:10.1073/pnas.1618475114
968 Socioeconomic Data and Applications Center (SEDAC). Retrieved from
969 https://sedac.ciesin.columbia.edu (accessed on September 23, 2020).
970 Thackray, C. P., Friedman, C. L., Zhang, Y. X., & Selin, N. E. (2015). Quantitative Assessment
971 of Parametric Uncertainty in Northern Hemisphere PAH Concentrations. *Environmental*
972 *Science & Technology*, *49*(15), 9185-9193. doi:10.1021/acs.est.5b01823
973 Thyssen, J., Althoff, J., Kimmerle, G., & Mohr, U. (1981). Inhalation studies with benzo[a]
974 pyrene in syrian golden-hamsters. *Journal of the National Cancer Institute*, *66*(3), 575-
975 577.
976 Travis, K. R., Jacob, D. J., Fisher, J. A., Kim, P. S., Marais, E. A., Zhu, L., . . . Zhou, X. L.
977 (2016). Why do models overestimate surface ozone in the Southeast United States?
978 *Atmospheric Chemistry and Physics*, *16*(21), 13561-13577. doi:10.5194/acp-16-13561-
979 2016
980 van Donkelaar, A., Martin, R. V., Leaitch, W. R., Macdonald, A. M., Walker, T. W., Streets, D.
981 G., . . . Andreae, M. O. (2008). Analysis of aircraft and satellite measurements from the
982 Intercontinental Chemical Transport Experiment (INTEX-B) to quantify long-range
983 transport of East Asian sulfur to Canada. *Atmospheric Chemistry and Physics*, *8*(11),
984 2999-3014. doi:10.5194/acp-8-2999-2008
985 Wesely, M. L. (1989). Parameterization of surface resistances to gaseous dry deposition in
986 regional-scale numerical-models. *Atmospheric Environment*, *23*(6), 1293-1304.
987 doi:10.1016/0004-6981(89)90153-4
988 Wilson, J. (2020). Modeling the Formation, Degradation, and Spatiotemporal Distribution of 2-
989 Nitrofluoranthene in the Global Atmosphere. *Environ Sci Technol* 54, 14224−14234.
990 Wislocki, P. G., Bagan, E. S., Lu, A. Y. H., Dooley, K. L., Fu, P. P., Hanhsu, H., . . . Kadlubar,
991 F. F. (1986). Tumorigenicity of nitrated derivatives of pyrene, benz[a]anthracene,
992 chrysene and benzo[a]pyrene in the newborn mouse assay. *Carcinogenesis*, *7*(8), 1317-
993 1322. doi:10.1093/carcin/7.8.1317
994 Zelenov, V. V., Aparina, E. V., Kozlovskiy, V. I., Sulimenkov, I. V., & Nosyrev, A. E. (2018).
995 Kinetics of NO_3 Uptake on Pyrene as a Representative Organic Aerosols. *Russian*
996 *Journal of Physical Chemistry B*, *12*(2), 343-351. doi:10.1134/s1990793118020136
997 Zhang, J., Li, J. Y., Wang, P., Chen, G., Mendola, P., Sherman, S., & Ying, Q. (2017).
998 Estimating population exposure to ambient polycyclic aromatic hydrocarbon in the
999 United States - Part I: Model development and evaluation. *Environment International*, *99*,
1000 263-274. doi:10.1016/j.envint.2016.12.002
1001 Zhang, J., Wang, P., Li, J. Y., Mendola, P., Sherman, S., & Ying, Q. (2016). Estimating
1002 population exposure to ambient polycyclic aromatic hydrocarbon in the United States -
1003 Part II: Source apportionment and cancer risk assessment. *Environment International*, *97*,
1004 163-170. doi:10.1016/j.envint.2016.08.024
1005 Zhang, L. M., Gong, S. L., Padro, J., & Barrie, L. (2001). A size-segregated particle dry
1006 deposition scheme for an atmospheric aerosol module. *Atmospheric Environment*, *35*(3),
1007 549-560. doi:10.1016/s1352-2310(00)00326-5

Zhang, P., Sun, W. Q., Li, N. N., Wang, Y. F., Shu, J. N., Yang, B., & Dong, L. (2014). Effects of Humidity and NO_3/N_2O_5 Ratio on the Heterogeneous Reaction of Fluoranthene and Pyrene with $N_2O_5/NO_3/NO_2$. *Environmental Science & Technology, 48*(22), 13130-13137. doi:10.1021/es504508v

Zhang, Y. X., Tao, S., Shen, H. Z., & Ma, J. M. (2009). Inhalation exposure to ambient polycyclic aromatic hydrocarbons and lung cancer risk of Chinese population. *Proceedings of the National Academy of Sciences of the United States of America, 106*(50), 21063-21067. doi:10.1073/pnas.0905756106

Zhou, S., Hwang, B. C. H., Lakey, P. S. J., Zuend, A., Abbatt, J. P. D., & Shiraiwa, M. (2019). Multiphase reactivity of polycyclic aromatic hydrocarbons is driven by phase separation and diffusion limitations. *Proceedings of the National Academy of Sciences of the United States of America, 116*(24), 11658-11663. doi:10.1073/pnas.1902517116

Zhou, S. M., Shiraiwa, M., McWhinney, R. D., Poschl, U., & Abbatt, J. P. D. (2013). Kinetic limitations in gas-particle reactions arising from slow diffusion in secondary organic aerosol. *Faraday Discussions, 165*, 391-406. doi:10.1039/c3fd00030c